Schweizerischer Erdbebendienst
Service Sismologique Suisse
Servizio Sismico Svizzero
Swiss Seismological Service

ETH zürich

Basel - St Johannspark (SBAJ2)

SITE CHARACTERIZATION REPORT

Clotaire MICHEL, Jan BURJANEK, Manuel HOBIGER

Valerio POGGI, Carlo CAUZZI, Donat FÄH

Sonneggstrasse 5 CH-8092 Zürich Switzerland; E-mail: clotaire.michel@sed.ethz.ch

Last modified : July 15, 2015

Abstract

Ambient vibration array measurements from a former project were reprocessed to characterize the site Basel St Johannspark. The site, where the new station SBAJ2 of the Swiss Strong Motion Network was installed, is located on an lower alluvial terrace of the Rhine in the city of Basel. The new station was installed in the frame of the Basel Erdbebenvorsorge project. In order to characterize the velocity profile under the station, existing array measurements with $230\,\mathrm{m}$ aperture were reprocessed. The analyses were successful and allowed deriving a velocity model for this site. The soil column underlying station SBAJ2 is made of a first layer of approximately $5\,\mathrm{m}$ with velocities from 180 to $300\,\mathrm{m/s}$ corresponding to anthropogenic infill and/or recent fluvial sediments. From 5 to $50\,\mathrm{m}$, the inversion gives velocities in the Septarienton formation (mudstone) of $480\,\mathrm{m/s}$. Another sharp interface is found at $130\,\mathrm{m}$ depth, within the Septarienton formation. The velocity reaches rapidly $1300\,\mathrm{m/s}$ below this interface and remains relatively constant down to the bedrock, found at $430\,\mathrm{m}$. It is producing the fundamental peak in the ellipticity at $0.75\,\mathrm{Hz}$.
$V_{s,30}$ is $410\,\mathrm{m/s}$, which would correspond to ground type B in the Eurocode 8 [CEN, 2004] and ground type C for the SIA261 [SIA, 2014]. The theoretical 1D SH transfer function computed from the inverted profiles shows amplifications up to a factor 3 at some resonance frequencies and match reasonably well the observed amplification at the station during earthquakes.

Contents

1 Introduction **4**

2 Geology **5**

3 Experiment description **5**

3.1 Ambient Vibrations 5

3.2 Equipment 5

3.3 Geometry of the arrays 6

3.4 Positioning of the stations 6

4 Data quality **7**

4.1 Usable data 7

4.2 Data processing 7

5 H/V processing **8**

5.1 Processing method and parameters 8

5.2 Results 8

5.3 Polarization analysis 11

6 Array processing **12**

6.1 Processing methods and parameters 12

6.2 Obtained dispersion curves 12

7 Inversion and interpretation **15**

7.1 Inversion 15

7.2 Travel time average velocities and ground type 19

7.3 SH transfer function and quarter-wavelength velocity 19

8 Conclusions **22**

References **24**

1 Introduction

The station SBAJ2 (Basel - St Johannspark) is part of the dense array of the Swiss Strong Motion Network (SSMNet) in Basel. SBAJ2 has been installed in the framework of the Basel Erdbebenvorsorge project in 2013 as a replacement for dial-up station SBAJ, located $40\,\mathrm{m}$ away to the NW. This project also includes the site characterization. Passive array measurements have been selected as a standard tool to investigate these sites. An array measurement campaign has been carried out in 2005 in St Johannspark by H.-B. Havenith in the frame of the INTERREG III project (Fig. 1), with a centre located $100\,\mathrm{m}$ away from SBAJ2 to the NW. These data have been reprocessed in order to characterize the velocity profile under this station. This station is located on a lower alluvial terrace of the Rhine. This report presents the measurement setup, the results of the H/V analysis and of the array processing of the surface waves (dispersion curves). Then, an inversion of these results into velocity profiles is performed. Standard parameters are derived to evaluate the amplification at this site.

Canton	City	Location	Station code	Site type	Slope
Basel Stadt	Basel	St Johannspark	SBAJ2	Alluvial terrace	Nearly flat

Table 1: Main characteristics of the study-site.

Figure 1: Picture of the site.

2 Geology

The station is located within the deep Rhine graben where resonance from Tertiary and Quaternary sediments is expected. The geological map indicates that the St Johannspark is located on a lower alluvial terrace of the Rhine (Pleistocene). In its eastern part, it is going down to the Rhine river following a gentle slope (about $10\,\mathrm{m}$ denivellation). Parts of the park include man-made infill. It should be noticed that the deep borehole called St Johann, performed in the frame of the Deep Heat Mining project is located too far (more than $1\,\mathrm{km}$ to the NW) to be used here. The terrace is approximately $23\,\mathrm{m}$ thick and lays on the Septarienton formation (formerly known as Meletta layers, a calcareous mudstone of Rupelian age, Tertiary). According to previous studies, the velocity contrast between these two layers that can be both regarded as stiff sediments, is however not very strong. Other Rupelian marl layers (from 25 up to $90\,\mathrm{m}$ thickness) are present below the Septarienton formation forming all together the "series grises". They are made of the sequence (from top to bottom): Fischschiefer (schist of 7 to $12\,\mathrm{m}$ thickness), Foraminifermergel (marl of 12 to $58\,\mathrm{m}$ thickness) and Meeressand (sandstone of 0 to $33\,\mathrm{m}$ thickness). According to the geological model of Basel, the Sannoisian marl (known as Haustein, also from Rupelian age), previously assumed as the geophysical bedrock, can be found at $240\,\mathrm{m}$ depth. Based on the Otterbach 2 VSP study, the geophysical basement is expected to be the Mesozoic limestone. Interpolations from the geological model lead to a depth of $420\,\mathrm{m}$ for this layer.

3 Experiment description

3.1 Ambient Vibrations

The ground surface is permanently subjected to ambient vibrations due to:

- natural sources (ocean and large-scale atmospheric phenomena) below $1\,\mathrm{Hz}$,
- local meteorological conditions (wind and rain) at frequencies around $1\,\mathrm{Hz}$,
- human activities (industrial machines, traffic…) at frequencies above $1\,\mathrm{Hz}$ [Bonnefoy-Claudet et al., 2006].

The objective of the measurements is to record these ambient vibrations and to use their propagation properties to infer the underground structure. First, the polarization of the recorded waves (H/V ratio) is used to derive the resonance frequencies of the soil column. Second, the arrival time delays at many different stations are used to derive the velocity of surface waves at different frequencies (dispersion). The information (H/V, dispersion curves) is then used to derive the properties of the soil column using an inversion process.

3.2 Equipment

For these measurements 4 Quanterra Q330 dataloggers named NR1 to NR4 and 7 Lennartz 3C 5 s seismometers were used (see Tab. 2). Each datalogger can record on 2 ports A (channels EH1, EH2, EH3 for Z, N, E directions) and B (channels EH4, EH5, EH6 for Z, N, E directions). Time synchronization was ensured by GPS.

Digitizer	Model	Number	Resolution
	Quanterra Q330	4	24 bits
Sensor type	**Model**	**Number**	**Cut-off frequency**
Velocimeter	Lennartz 3C	7	0.2 Hz

Table 2: Equipment used.

3.3 Geometry of the arrays

Three array configurations have been performed, corresponding to 3 rings of 20, 50 and 115 m radius around a central station. Each configuration includes one ring with 6 sensors and the central station. The minimum inter-station distance and the aperture are therefore 20 and 40 m, 50 and 100 m and 115 and 230 m, respectively. The experimental setup is displayed in Fig. 2. The final usable datasets are detailed in section 4.2.

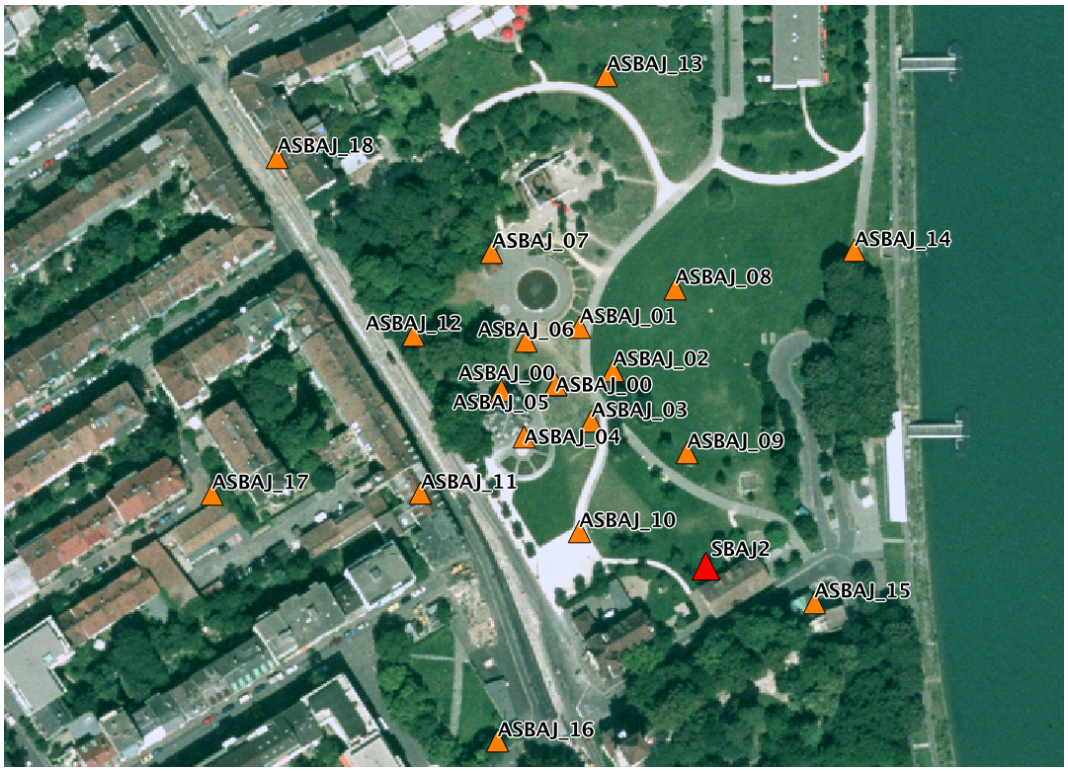

Figure 2: Geometry of the arrays.

3.4 Positioning of the stations

The sensor coordinates were measured using a theodolite. It allows a relative positioning with an accuracy of about 10 cm on the Swissgrid.

4 Data quality

4.1 Usable data

The largest time windows were extracted, for which all the sensors of the array were correctly placed and the GPS synchronization was ensured. Point ASBAJ_04 happens not to have recorded data and was removed from the analysis.

Orientations of the sensors were checked by maximizing the correlation with the central station at low frequencies [Poggi et al., 2012b]. Deviations lower than $8\,^\circ$ were found for all points but ASBAJ_18 ($11\,^\circ$), ASBAJ_14 ($12\,^\circ$), ASBAJ_17 ($17\,^\circ$) and especially ASBAJ_08 ($37\,^\circ$?!). Original and rotated datasets are available for the 3C array analysis.

The characteristics of the datasets are detailed in Tab. 3.

4.2 Data processing

The data were first converted to SAC format including in the header the coordinates of the point (CH1903 system), the recording component and a name related to the position. The name is made of 5 letters characterizing the location (ASBAJ_ here) and 2 digits for the point number from 00 to 18. Recordings were not corrected for the full instrumental response but only for a conversion factor, i.e. saved in m/s

Dataset	**Starting Date**	**Time**	**Length**	F_s	**Min. inter-distance**	**Aperture**	**# of points**
1	2005/02/18	10:16	52 min	200 Hz	20 m	40 m	6
2	2005/02/18	11:59	44 min	200 Hz	50 m	100 m	7
3	2005/02/18	13:35	44 min	200 Hz	115 m	230 m	7

Table 3: Usable datasets.

5 H/V processing

5.1 Processing method and parameters

In order to process the H/V spectral ratios, several codes and methods were used. The classical H/V method was applied using the Geopsy `http://www.geopsy.org` software. In this method, the ratio of the smoothed Fourier Transform of selected time windows are averaged. Tukey windows (cosine taper of 5% width) of $50\,\mathrm{s}$ long overlapping by 50% were selected. Konno and Ohmachi [1998] smoothing procedure was used with a b value of 60. The classical method computed using the method of Fäh et al. [2001] was also performed.

Moreover, the time-frequency analysis method [Fäh et al., 2009] was used to estimate the ellipticity function more accurately using the Matlab code of V. Poggi. In this method, the time-frequency analysis using the Wavelet transform is computed for each component. For each frequency, the maxima over time (10 per minute with at least $0.1\,\mathrm{s}$ between each) in the TFA are determined. The Horizontal to Vertical ratio of amplitudes for each maximum is then computed and statistical properties for each frequency are derived. A Cosine wavelet with parameter 9 is used. The mean of the distribution for each frequency is stored. For the sake of comparison, the time-frequency analysis of Fäh et al. [2001], based on the spectrogram, was also used.

The ellipticity extraction using the Capon analysis [Poggi and Fäh, 2010] (see section on array analysis) was also performed.

Method	Freq. band	Win. length	Anti-trig.	Overlap	Smoothing
Standard H/V Geopsy	$0.2 - 20\,\mathrm{Hz}$	$50\,\mathrm{s}$	No	50%	K&O 60
Standard H/V D. Fäh	$0.2 - 20\,\mathrm{Hz}$	$30\,\mathrm{s}$	No	75%	-
H/V TFA D. Fäh	$0.2 - 20\,\mathrm{Hz}$	Specgram	No	-	-
H/V TFA V. Poggi	$0.2 - 20\,\mathrm{Hz}$	Cosine wpar=9	No	-	No

Table 4: Methods and parameters used for the H/V processing.

5.2 Results

Although the right flank is the same for all points, the fundamental peak has 2 different shapes depending on the point. Most of the points show a double peak at 0.6 and $1\,\mathrm{Hz}$, the second being more prominent. Other points show a single wide peak at $0.75\,\mathrm{Hz}$. The previous experience of picking H/V curves in Basel tells that all curves should be considered as having only 1 large peak. Its value is therefore $0.75\,\mathrm{Hz}$ with an amplitude of 3 to 7 for TFA methods.

A second peak above $10\,\mathrm{Hz}$ can be noticed on all recordings, although sometimes at too high frequency or with low amplitude. This resonance frequency especially appears in the central part of the park and is at higher frequencies outside of the park. It corresponds to only several meters of loose sediments that are therefore very variable in this region with man-made infill and slope towards the Rhine river. At point ASBAJ_14, close to the river, this peak is at lower frequency ($8\,\mathrm{Hz}$) indicating the presence of a layer of about $10\,\mathrm{m}$, if one assumes a shear wave velocity of $200 - 400\,\mathrm{m/s}$.

It should be noticed that this peak is not observed in Fig. 4 on the test station XBA11 located close to the permanent station SBAJ2. On the accelerometric data of the permanent station, this peak is present at about $17\,\mathrm{Hz}$, but the amplitude is weak. Assuming a shear wave velocity of $200 - 400\,\mathrm{m/s}$, this would correspond to 3 to $6\,\mathrm{m}$ of surface sediments. On this plot, the low frequencies should not be considered since they are affected by the noise of the instrument. The temporary station XBA11 was located in the basement of a building, about $3\,\mathrm{m}$ below the permanent station, which explains this difference.

Moreover, all the methods to compute H/V ratios are compared at the array centre on Fig. 5, in which the classical methods were divided by $\sqrt{2}$ to correct from the Love wave contribution [Fäh et al., 2001]. The classical and TFA methods match well at high frequencies but large variations are observed at low frequencies, making the interpretation of the broad peak difficult. The 3C FK analysis (Capon method) does not have resolution down to the peak but matches perfectly with the H/V analysis at high frequency.

The fundamental peak at the SBAJ2 station is therefore at $0.75\,\mathrm{Hz}$, with a peak amplitude around 3 for the TFA methods. A small peak at $17\,\mathrm{Hz}$ is also present.

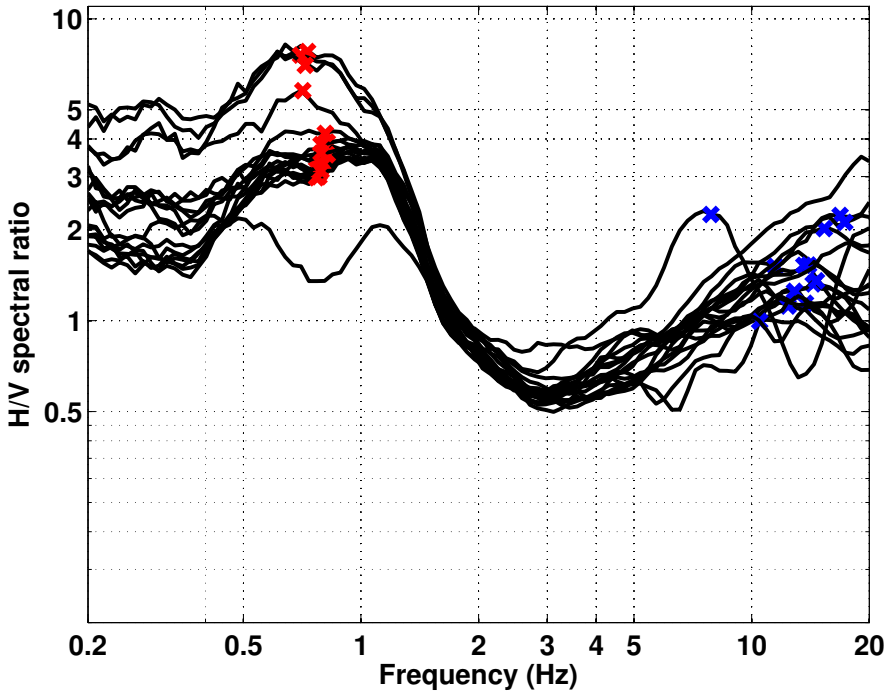

Figure 3: H/V spectral ratios (time-frequency analysis code V. Poggi) of all array points.

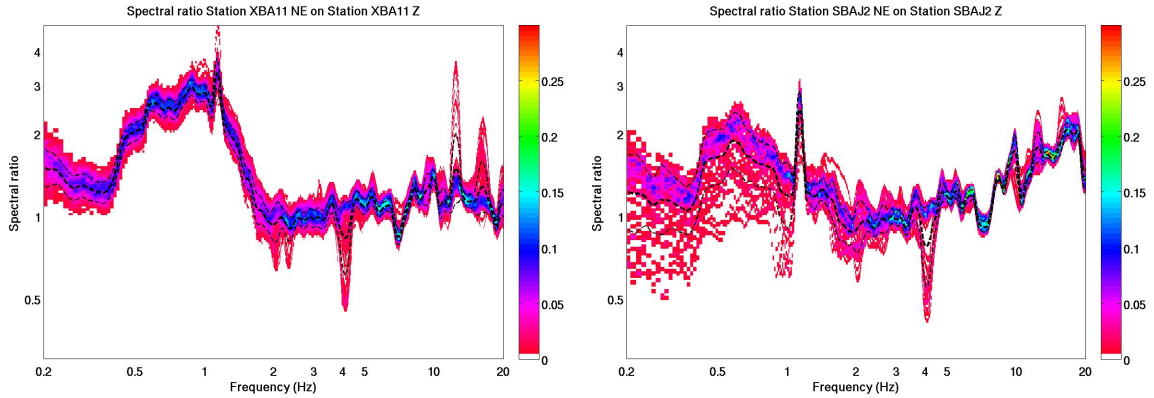

Figure 4: H/V spectral ratios (classical method) from the 1-week test station XBA11 (left) and the permanent accelerometric station SBAJ2 (right).

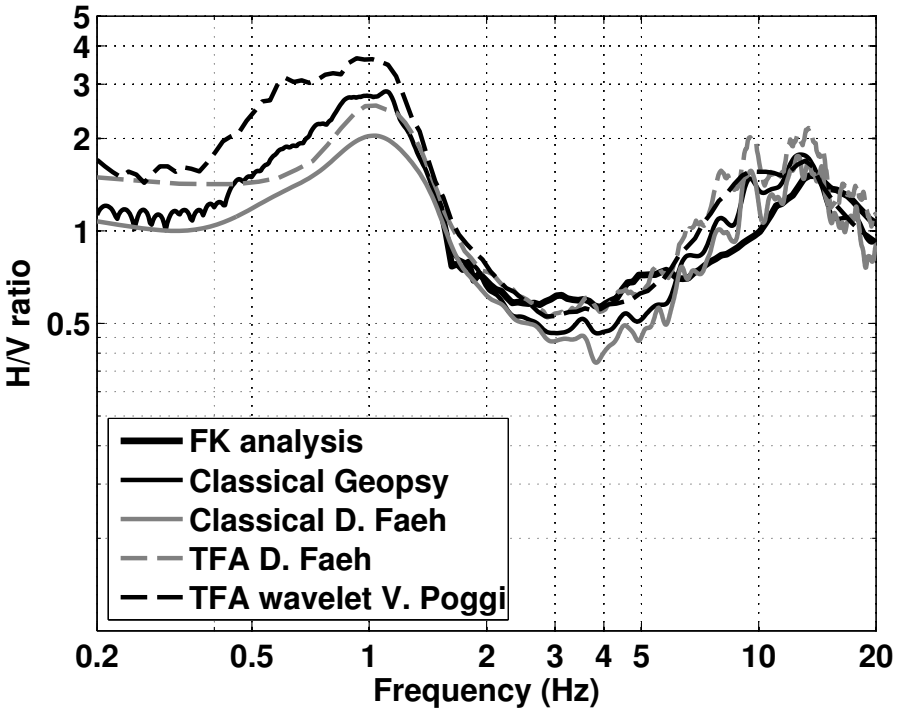

Figure 5: H/V spectral ratios for point ASBAJ_00 using the different codes. Classical methods were divided by $\sqrt{2}$.

5.3 Polarization analysis

Considering the shape of the Rhine basin, a 2D resonance could occur. Therefore, polarization analysis on the array data was performed using the method of Burjánek et al. [2010]. All points (Fig. 6) do not show any polarization at the resonance frequency. Polarization of the spurious peaks at 1.13 Hz is however clearly visible. No 2D resonance occurs at this location.

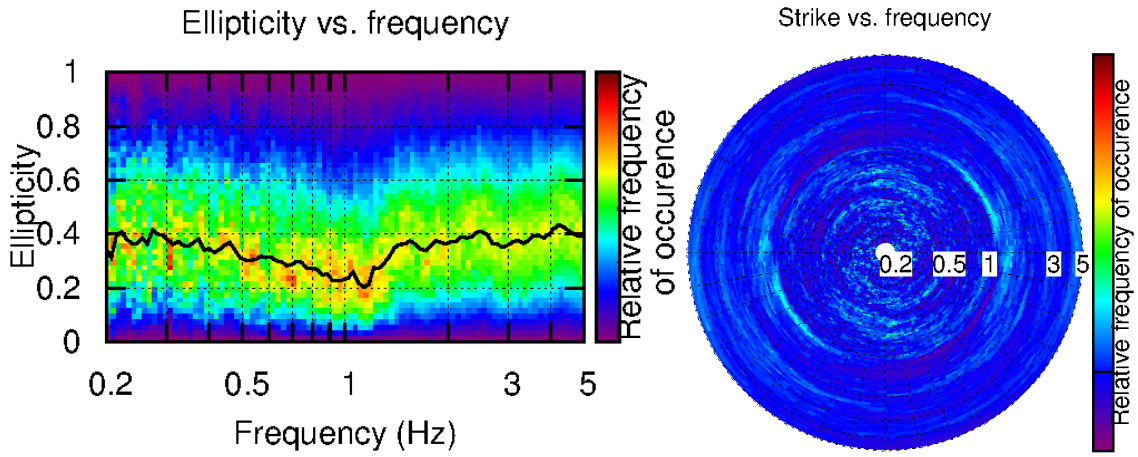

Figure 6: Polarization analysis at point ASBAJ_00. Left: Ellipticity (A trough in the ellipticity corresponds to polarized motion). Right: Strike of the polarization.

6 Array processing

6.1 Processing methods and parameters

The vertical components of the arrays were processed using the FK and the High-resolution FK analysis [Capon, 1969] using the Geopsy `http://www.geopsy.org` software. Better results were obtained using large time windows (300T). The results of computations of both datasets were merged to estimate the dispersion curves.

Moreover, a 3C array analysis [Fäh et al., 2008] was also performed using the array_tool_3C software [Poggi and Fäh, 2010]. It allows us to derive Rayleigh and Love modes including the Rayleigh ellipticity. The results of computations of both datasets were merged to estimate the dispersion curves.

Method	Set	Freq. band	Win. length	Anti-trig.	Overlap	Grid step	Grid size	# max.
HRFK 1C	1	$1-25\,\mathrm{Hz}$	$300T$	No	50%	0.001	0.6	5
HRFK 1C	2	$1-25\,\mathrm{Hz}$	$300T$	No	50%	0.001	0.6	5
HRFK 1C	3	$1-25\,\mathrm{Hz}$	$300T$	No	50%	0.001	0.6	5
HRFK 3C	1	$1-25\,\mathrm{Hz}$	Wav. 10	No	50%	300	2000	5
			Tap. 0.2			m/s	m/s	
HRFK 3C	2	$1-25\,\mathrm{Hz}$	Wav. 10	No	50%	300	2000	5
			Tap. 0.2			m/s	m/s	
HRFK 3C	3	$1-25\,\mathrm{Hz}$	Wav. 10	No	50%	300	2000	5
			Tap. 0.2			m/s	m/s	

Table 5: Methods and parameters used for the array processing.

6.2 Obtained dispersion curves

In the 1C FK analysis, the fundamental Rayleigh mode could be picked between 1.8 and $11.5\,\mathrm{Hz}$ (Fig. 7). The velocities range from $1000\,\mathrm{m/s}$ at $1.9\,\mathrm{Hz}$ down to $400\,\mathrm{m/s}$ at $12\,\mathrm{Hz}$.

Using the 3C analysis, the fundamental and a higher Rayleigh modes can be picked, although the higher mode is uncertain (Fig. 7). On the transverse component, the picked curve is uncertain (Fig. 8): below $3\,\mathrm{Hz}$ the spread is large, above $10\,\mathrm{Hz}$ the picking is questionable. The intermediate part could be the first higher mode.

All picked curves are presented together on Fig. 9. The fundamental, first and higher Rayleigh modes are identical for 1C and 3C analysis.

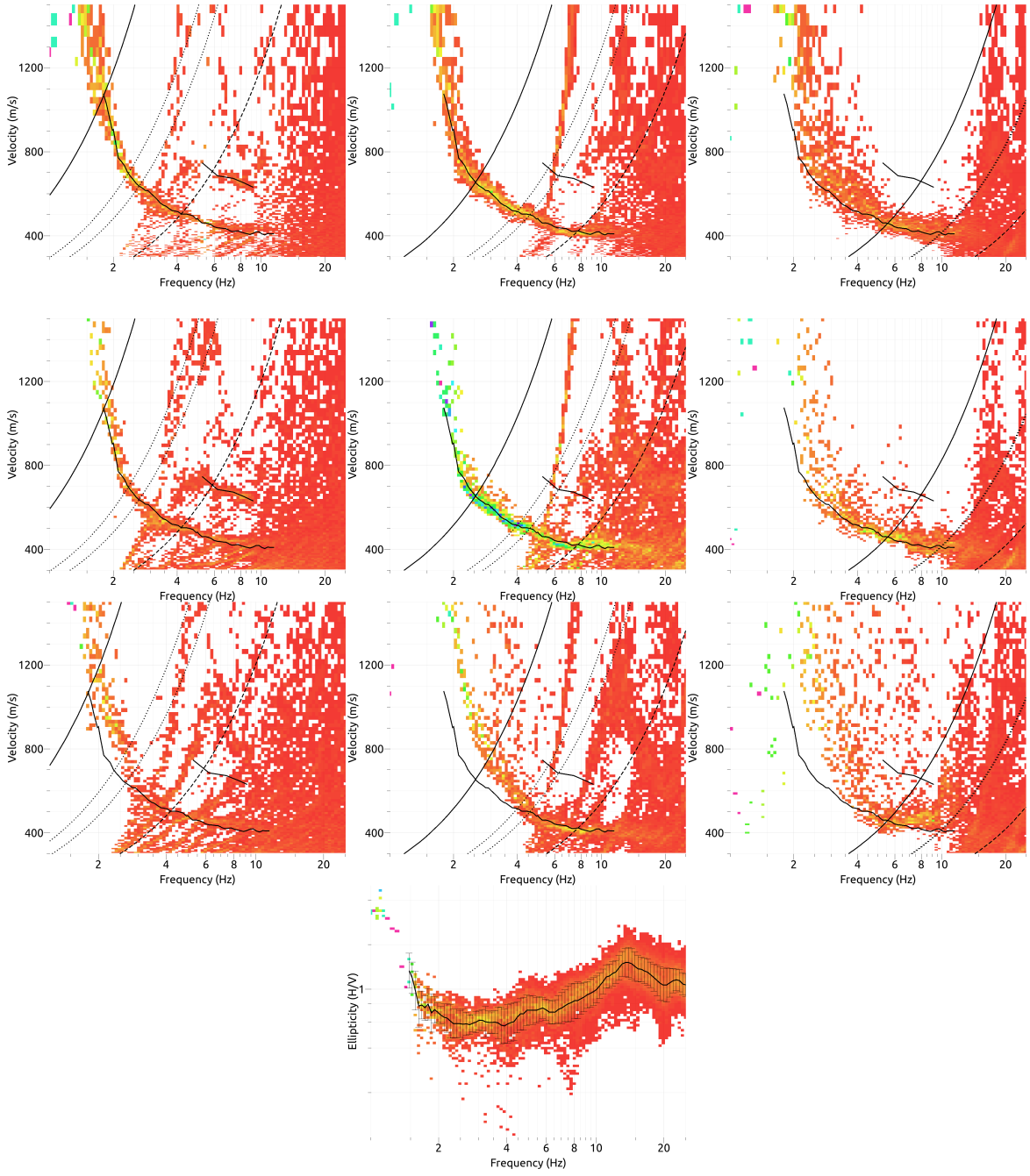

Figure 7: Dispersion curves and ellipticity obtained from the 1C and 3C array analyses for Rayleigh waves. From left to right: datasets 3, 2 and 1. First row: 1C vertical; second row: 3C vertical; third row: 3C radial; fourth row: ellipticity).

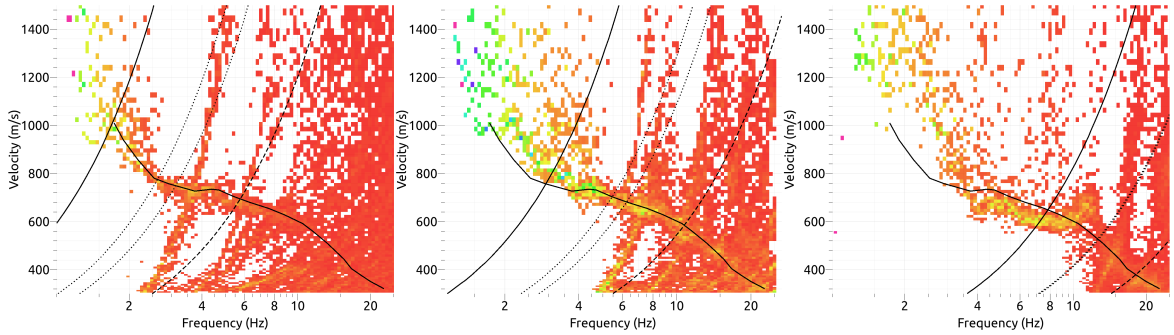

Figure 8: Dispersion curves for the transverse component of the 3C array analysis. From left to right: datasets 3, 2 and 1.

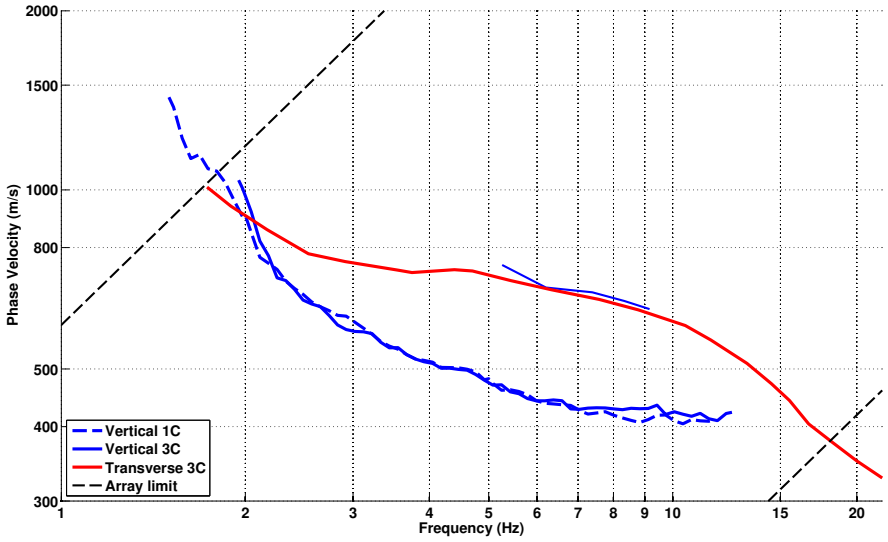

Figure 9: Picked dispersion curves from 1C and 3C FK methods.

7 Inversion and interpretation

7.1 Inversion

For the inversion, Rayleigh fundamental and first higher mode dispersion curves and the ellipticity curve were used as simultaneous targets without standard deviation. After many tests, the Love dispersion curve was discarded for this computation. This curve is not compatible with the other targets as a fundamental. Other inversions were also performed using the Love dispersion curve instead of Rayleigh but they do not provide realistic results. A weight of 0.5 was assigned to the ellipticity curve. All curves were resampled using 50 points between 0.4 and $25\,\mathrm{Hz}$ in log scale.

The inversion was performed using the Improved Neighborhood Algorithm (NA) [Wathelet, 2008] implemented in the Dinver software. In this algorithm, the tuning parameters are the following: Ns_0 is the number of starting models, randomly distributed in the parameter space, Nr is the the number of best cells considered around these Ns_0 models, Ns is the number of new cells generated in the neighborhood of the Nr cells (Ns/Nr per cell) and It_{max} is the number of iteration of this process. The process ends with $Ns_0 + Nr * \frac{Ns}{Nr} * It_{max}$ models. The used parameters are detailed in Tab. 6.

It_{max}	Ns_0	Ns	Nr
500	10000	100	100

Table 6: Tuning parameters of Neighborhood Algorithm.

No low velocity zones were allowed during the inversion. The Poisson ratio was inverted in each layer in the range 0.2-0.4, up to 0.47 jus below the groundwater table. The density was assumed to be $2000\,\mathrm{kg/m^3}$ in the sediments and $2700\,\mathrm{kg/m^3}$ in the Mesozoic rock. 4 layers are enough to explain most of the targets (dispersion and ellipticity), but more layers are used to smooth the obtained results and better explore the parameter space. 5 independent runs of 5 different parametrization schemes (6 and 7 layers over a half space and 10, 12 and 15 layers with fixed depth) were performed. Examples of retrieved ground profiles for these two strategies are presented in Fig. 10. When comparing to the target curves (Fig. 11), the Rayleigh fundamental and first higher modes are well represented, as well as the ellipticity. As explained above, the fundamental Love mode is not compatible with this velocity profile.

For further elaborations, the best models of these 25 runs were selected (Fig. 12). The first five meters of the profile show low velocities, from $180\,\mathrm{m/s}$, increasing rapidly. Below $5\,\mathrm{m}$ depth, the velocity is relatively constant around $480\,\mathrm{m/s}$ down to approximately $50\,\mathrm{m}$. No contrast between Quaternary and Tertiary sediments at $23\,\mathrm{m}$ depth can be seen. At $50\,\mathrm{m}$ depth, a sharp contrast is clearly seen with velocity jumping up to about $700\,\mathrm{m/s}$. In previous work, the first $50\,\mathrm{m}$ with low velocities are interpreted as weathered Tertiary rock and can be seen everywhere in Basel with slightly varying depths. Another sharp interface is found at $130\,\mathrm{m}$ depth. It most probably occurs within the Septarienton formation, though it could be the interface with the Fischschiefer. The velocity reaches rapidly $1300\,\mathrm{m/s}$ below this interface and remains relatively constant down to the bedrock. Finally, the bedrock is found between 415 and $480\,\mathrm{m}$ depth ($430\,\mathrm{m}$ on average), as expected.

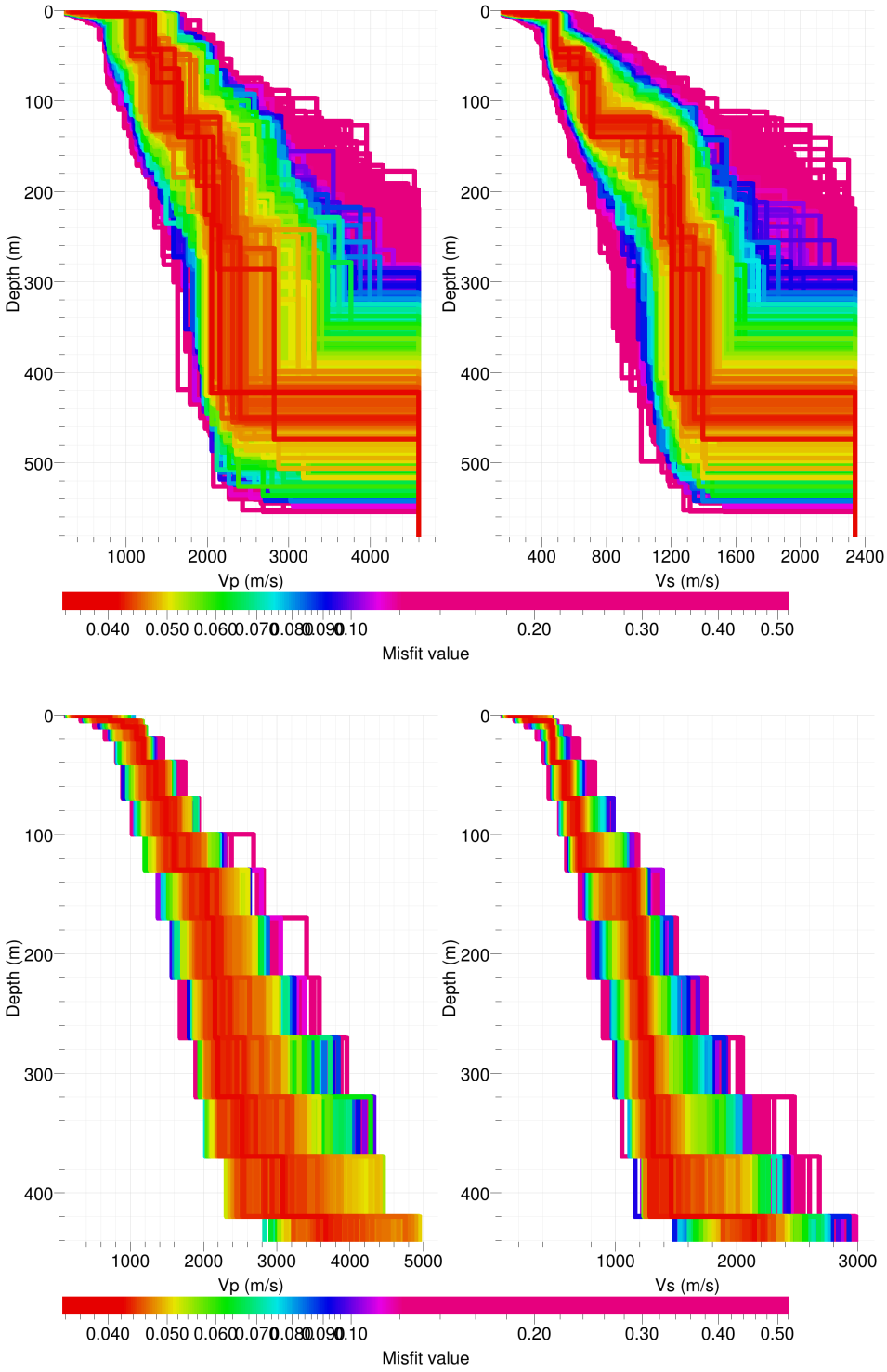

Figure 10: Inverted ground profiles in terms of V_p and V_s; top: free layer depth strategy; bottom: fixed layer depth strategy.

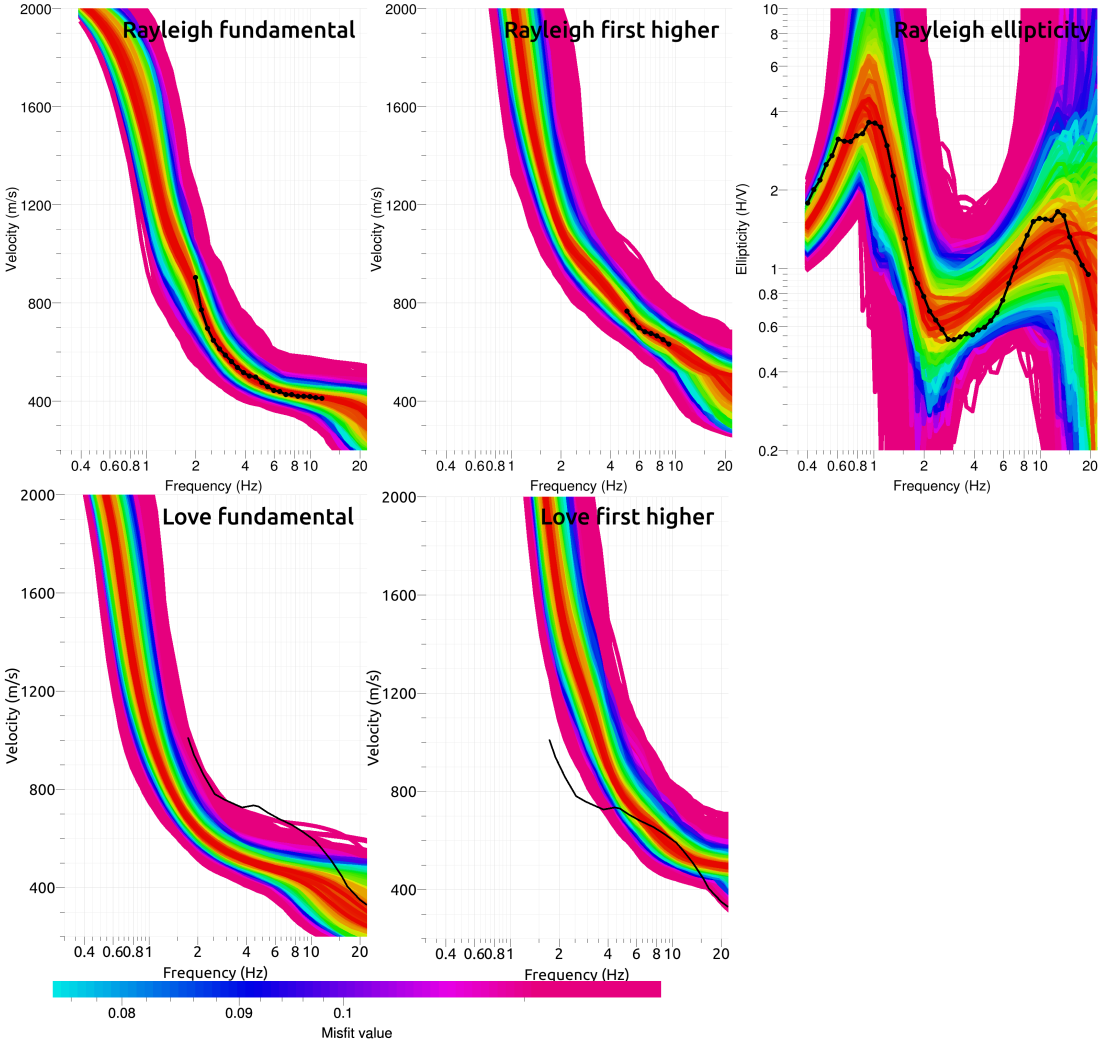

Figure 11: Comparison between inverted models and measured Rayleigh and Love modes and corresponding ellipticity. Thin black lines were not used in the inversion.

The comparison with the models derived by Havenith and Fäh [2006] using the same data and the 3D numerical model of Basel [Opršal et al., 2005] (Fig. 12) shows a good agreement in the upper part, though the previous authors tried to resolve more details in the profiles. The blue profiles loose their resolution at $150\,\mathrm{m}$, on the contrary to our study where the inversion is pushed to lower frequencies, constrained by the ellipticity. Havenith and Fäh [2006] were assuming a geophysical bedrock at $200\,\mathrm{m}$ that did not allow to reproduce the ellipticity curve. The 3D model followed the same assumption, leading to an incorrect velocity profile below $150\,\mathrm{m}$.

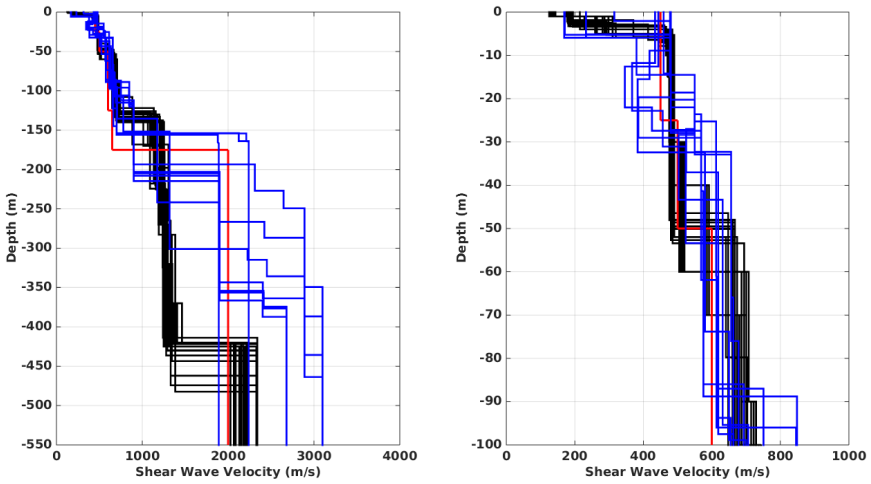

Figure 12: V_s ground profiles for the selected 25 best models (black) compared to the models derived by Havenith and Fäh [2006] (blue) and the 3D numerical model of Basel [Opršal et al., 2005] (red).

7.2 Travel time average velocities and ground type

The distribution of the travel time average velocities at different depths was computed from the selected models. The uncertainty, computed as the standard deviation of the distribution of travel time average velocities for the considered models, is also provided, but its meaning is doubtful. $V_{s,30}$ is found to be $410\,\mathrm{m/s}$, which corresponds to class B in the Eurocode 8 [CEN, 2004] and class C in the SIA261 [SIA, 2014].

	Mean (m/s)	**Uncertainty (m/s)**
$V_{s,5}$	236	14
$V_{s,10}$	314	12
$V_{s,20}$	380	9
$V_{s,30}$	410	8
$V_{s,40}$	427	7
$V_{s,50}$	442	8
$V_{s,100}$	529	5
$V_{s,150}$	598	4
$V_{s,200}$	681	5

Table 7: Travel time averages at different depths from the inverted models. Uncertainty is given as one standard deviation from the selected profiles.

7.3 SH transfer function and quarter-wavelength velocity

The quarter-wavelength velocity approach [Joyner et al., 1981] provides, for a given frequency, the average velocity at a depth corresponding to 1/4 of the wavelength of interest. It is useful to identify the frequency limits of the experimental data (minimum frequency in dispersion curves at $1.8\,\mathrm{Hz}$ and in the ellipticity at $0.75\,\mathrm{Hz}$ here). The results using this proxy show that the dispersion curves constrain the profiles down to $70\,\mathrm{m}$ and the ellipticity down to $250\,\mathrm{m}$ (Fig. 13). Moreover, the quarter wavelength impedance-contrast introduced by Poggi et al. [2012a] is also displayed in the figure. It corresponds to the ratio between two quarter-wavelength average velocities, respectively from the top and the bottom part of the velocity profile, at a given frequency [Poggi et al., 2012a]. It shows a trough (inverse shows a peak) at the resonance frequency.

Moreover, the theoretical SH-wave transfer function for vertical propagation [Roesset, 1970] is computed from the inverted profiles. It is corrected with respect to the Swiss Reference Rock model [Poggi et al., 2011] following Edwards et al. [2013]. In this case, the models are predicting an amplification up to a facMesozoictor of 3 at several resonance peaks. The comparison with the Empirical Spectral Modeling (ESM) amplification obtained from earthquake recordings [Edwards et al., 2013] shows a reasonable agreement.

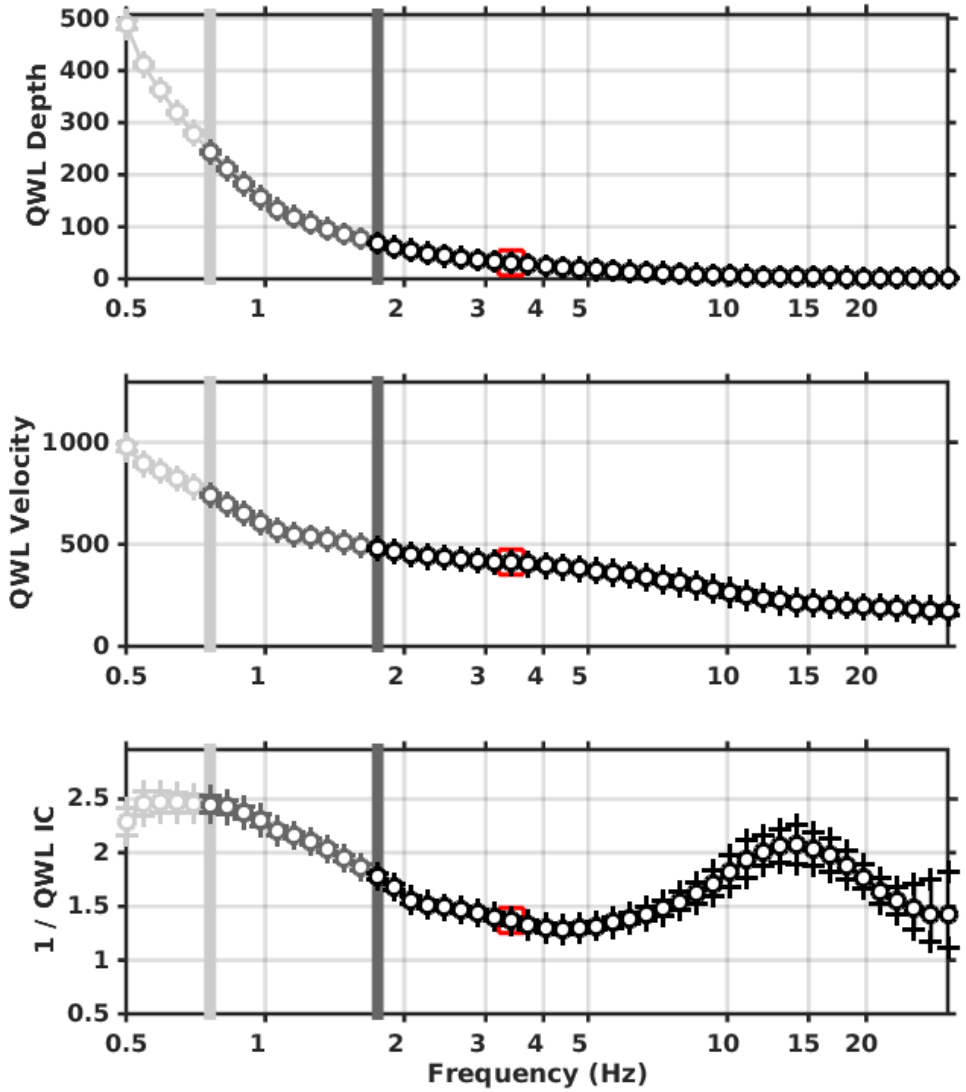

Figure 13: Quarter wavelength velocity representation of the velocity profile (top: depth, centre: velocity, bottom: inverse of the impedance contrast). Black curve is constrained by the dispersion curves, light grey is not constrained by the data. Red square is corresponding to $V_{s,30}$.

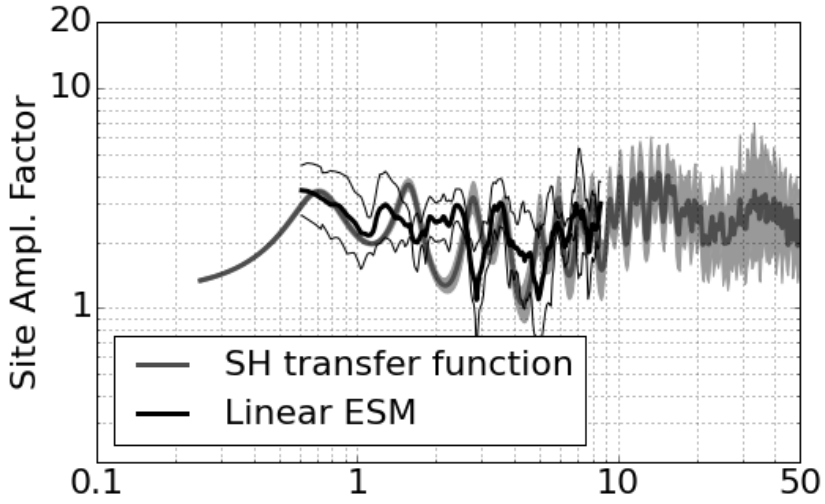

Figure 14: Theoretical SH transfer function (grey line) compared to the empirical spectral amplification [Edwards et al., 2013] (black line) with its standard deviation. Both are referenced at the Swiss Reference Rock Model [Poggi et al., 2011].

8 Conclusions

Using existing array data, we derived new velocity models for the site of the SBAJ2 station. We found a first layer of approximately $5\,\mathrm{m}$ with velocities from 180 to $300\,\mathrm{m/s}$ corresponding to anthropogenic infill and/or recent fluvial sediments. From 5 to $50\,\mathrm{m}$, the inversion gives velocities in the Septarienton formation (mudstone) of $480\,\mathrm{m/s}$. Another sharp interface is found at $130\,\mathrm{m}$ depth, within the Septarienton formation. The velocity reaches rapidly $1300\,\mathrm{m/s}$ below this interface and remains relatively constant down to the bedrock, found at $430\,\mathrm{m}$. It is producing the fundamental peak in the ellipticity at $0.75\,\mathrm{Hz}$.
$V_{s,30}$ is $410\,\mathrm{m/s}$, which would correspond to ground type B in the Eurocode 8 [CEN, 2004] and ground type C for the SIA261 [SIA, 2014]. The theoretical 1D SH transfer function computed from the inverted profiles shows amplifications up to a factor 3 at some resonance frequencies and match reasonably well the observed amplification at the station during earthquakes.

Acknowledgements

The authors thank HB Havenith who performed the measurements.

References

Sylvette Bonnefoy-Claudet, Fabrice Cotton, and Pierre,ÄêYves Bard. The nature of noise wavefield and its applications for site effects studies. *Earth-Science Reviews*, 79(3-4): 205–227, December 2006. ISSN 00128252. doi: 10.1016/j.earscirev.2006.07.004. URL http://linkinghub.elsevier.com/retrieve/pii/S0012825206001012.

Jan Burjánek, Gabriela Gassner-Stamm, Valerio Poggi, Jeffrey R. Moore, and Donat Fäh. Ambient vibration analysis of an unstable mountain slope. *Geophysical Journal International*, 180(2):820–828, February 2010. ISSN 0956540X. doi: 10.1111/j.1365-246X.2009.04451.x. URL http://gji.oxfordjournals.org/cgi/doi/10.1111/j.1365-246X.2009.04451.xhttp://doi.wiley.com/10.1111/j.1365-246X.2009.04451.x.

J. Capon. High-Resolution Frequency-Wavenumber Spectrum Analysis. *Proceedings of the IEEE*, 57(8):1408–1418, 1969. ISSN 0018-9219. doi: 10.1109/PROC.1969.7278. URL http://ieeexplore.ieee.org/lpdocs/epic03/wrapper.htm?arnumber=1449208.

CEN. *Eurocode 8: Design of structures for earthquake resistance - Part 1: General rules, seismic actions and rules for buildings*. European Committee for Standardization, en 1998-1: edition, 2004.

Benjamin Edwards, Clotaire Michel, Valerio Poggi, and Donat Fäh. Determination of Site Amplification from Regional Seismicity : Application to the Swiss National Seismic Networks. *Seismological Research Letters*, 84(4), 2013. doi: 10.1785/0220120176.

Donat Fäh, Fortunat Kind, and Domenico Giardini. A theoretical investigation of average H/V ratios. *Geophysical Journal International*, 145(2):535–549, May 2001. ISSN 0956540X. doi: 10.1046/j.0956-540x.2001.01406.x. URL http://doi.wiley.com/10.1046/j.0956-540x.2001.01406.x.

Donat Fäh, Gabriela Stamm, and Hans-Balder Havenith. Analysis of three-component ambient vibration array measurements. *Geophysical Journal International*, 172(1):199–213, January 2008. ISSN 0956540X. doi: 10.1111/j.1365-246X.2007.03625.x. URL http://doi.wiley.com/10.1111/j.1365-246X.2007.03625.xhttp://gji.oxfordjournals.org/cgi/doi/10.1111/j.1365-246X.2007.03625.x.

Donat Fäh, Marc Wathelet, Miriam Kristekova, Hans-Balder Havenith, Brigitte Endrun, Gabriela Stamm, Valerio Poggi, Jan Burjánek, and Cécile Cornou. Using Ellipticity Information for Site Characterisation. Technical report, NERIES JRA4 Task B2, 2009.

Hans-Balder Havenith and Donat Fäh. INTERREG III Projekt: Erdbebenmikrozonierung am südlichen Oberrhein. Teilbericht 2: Bestimmung der Scherwellengeschwindigkeiten. Technical report, Eidgenössische Technische Hochschule Zürich (ETHZ), 2006.

William B. Joyner, Richard E. Warrick, and Thomas E. Fumal. The effect of Quaternary alluvium on strong ground motion in the Coyote Lake, California, earthquake of 1979. *Bulletin of the Seismological Society of America*, 71(4):1333–1349, 1981.

Katsuaki Konno and Tatsuo Ohmachi. Ground-Motion Characteristics Estimated from Spectral Ratio between Horizontal and Vertical Components of Microtremor. *Bulletin of the Seismological Society of America*, 88(1):228–241, 1998.

Ivo Opršal, Donat Fäh, P. Martin Mai, and Domenico Giardini. Deterministic earthquake scenario for the Basel area: Simulating strong motions and site effects for Basel, Switzerland. *Journal of Geophysical Research*, 110(B4):1–19, 2005. ISSN 0148-0227. doi: 10.1029/2004JB003188. URL http://doi.wiley.com/10.1029/2004JB003188http://www.agu.org/pubs/crossref/2005/2004JB003188.shtml.

Valerio Poggi and Donat Fäh. Estimating Rayleigh wave particle motion from three-component array analysis of ambient vibrations. *Geophysical Journal International*, 180(1):251–267, January 2010. ISSN 0956540X. doi: 10.1111/j.1365-246X.2009.04402.x. URL http://doi.wiley.com/10.1111/j.1365-246X.2009.04402.x.

Valerio Poggi, Benjamin Edwards, and Donat Fäh. Derivation of a Reference Shear-Wave Velocity Model from Empirical Site Amplification. *Bulletin of the Seismological Society of America*, 101(1):258–274, January 2011. ISSN 0037-1106. doi: 10.1785/0120100060. URL http://www.bssaonline.org/cgi/doi/10.1785/0120100060.

Valerio Poggi, Benjamin Edwards, and Donat Fäh. Characterizing the Vertical-to-Horizontal Ratio of Ground Motion at Soft-Sediment Sites. *Bulletin of the Seismological Society of America*, 102(6):2741–2756, December 2012a. ISSN 0037-1106. doi: 10.1785/0120120039. URL http://www.bssaonline.org/cgi/doi/10.1785/0120120039.

Valerio Poggi, Donat Fäh, Jan Burjánek, and Domenico Giardini. The use of Rayleigh-wave ellipticity for site-specific hazard assessment and microzonation: application to the city of Lucerne, Switzerland. *Geophysical Journal International*, 188(3):1154–1172, March 2012b. ISSN 0956540X. doi: 10.1111/j.1365-246X.2011.05305.x. URL http://doi.wiley.com/10.1111/j.1365-246X.2011.05305.xhttp://gji.oxfordjournals.org/cgi/doi/10.1111/j.1365-246X.2011.05305.x.

J.M. Roesset. Fundamentals of soil amplification. In R. J. Hansen, editor, *Seismic Design for Nuclear Power Plants*, pages 183–244. M.I.T. Press, Cambridge, Mass., 1970. ISBN 978-0-262-08041-5. URL http://mitpress.mit.edu/catalog/item/default.asp?ttype=2&tid=5998.

SIA. *SIA 261 Einwirkungen auf Tragwerke*. Société suisse des ingénieurs et des architectes, Zurich, Switzerland, 2014.

Marc Wathelet. An improved neighborhood algorithm: Parameter conditions and dynamic scaling. *Geophysical Research Letters*, 35(9):1–5, May 2008. ISSN 0094-8276. doi: 10.1029/2008GL033256. URL http://www.agu.org/pubs/crossref/2008/2008GL033256.shtml.